2011

A Keck LGS AO search for brown dwarf and planetary mass companions to upper Scorpius brown dwarfs

B. Biller

Katelyn N. Allers
Bucknell University, kna003@bucknell.edu

Michael Liu

Laird Close

Trent Dupuy

Follow this and additional works at: https://digitalcommons.bucknell.edu/fac_journ

Part of the Astrophysics and Astronomy Commons

Recommended Citation

A KECK LGS AO SEARCH FOR BROWN DWARF AND PLANETARY MASS COMPANIONS TO UPPER SCORPIUS BROWN DWARFS

Beth Biller[1,4,5], Katelyn Allers[2], Michael Liu[1], Laird M. Close[3], and Trent Dupuy[1,5,6]
[1] Institute for Astronomy, University of Hawaii, 2680 Woodlawn Drive, Honolulu, HI 96822, USA
[2] Department of Physics and Astronomy, 153 Olin Science, Bucknell University, Lewisburg, PA 17837, USA
[3] Steward Observatory, University of Arizona, 933 North Cherry Avenue, Tucson, AZ 85721, USA

ABSTRACT

We searched for binary companions to 20 young brown dwarfs in the Upper Scorpius association (145 pc, 5 Myr, nearest OB association) with the Laser Guide Star adaptive optics system and the facility infrared camera NIRC2 on the 10 m Keck II telescope. We discovered a $0\rlap{.}''14$ companion (20.9 ± 0.4 AU) to the $<0.1\,M_\odot$ object SCH J16091837−20073523. From spectral deconvolution of integrated-light near-IR spectroscopy of SCH1609 using the SpeX spectrograph (Rayner et al. 2003), we estimate primary and secondary spectral types of M6 ± 0.5 and M7 ± 1.0, corresponding to masses of 79 ± 17 $M_{\rm Jup}$ and 55 ± 25 $M_{\rm Jup}$ at an age of 5 Myr and masses of 84 ± 15 $M_{\rm Jup}$ and 60 ± 25 $M_{\rm Jup}$ at an age of 10 Myr. For our survey objects with spectral types later than M8, we find an upper limit on the binary fraction of <9% (1σ) at separations of 10–500 AU. We combine the results of our survey with previous surveys of Upper Sco and similar young regions to set the strongest constraints to date on binary fraction for young substellar objects and very low mass stars. The binary fraction for low-mass ($<40\,M_{\rm Jup}$) brown dwarfs in Upper Sco is similar to that for T dwarfs in the field; for higher mass brown dwarfs and very low mass stars, there is an excess of medium-separation (10–50 AU projected separation) young binaries with respect to the field. These medium-separation binaries will likely survive to late ages.

Key words: binaries: general – brown dwarfs – stars: low-mass – stars: pre-main sequence

Online-only material: color figures

1. INTRODUCTION

Numerous brown dwarf binaries have been discovered in the field (Close et al. 2003; Burgasser et al. 2003; Bouy et al. 2003; Burgasser et al. 2006; Liu et al. 2006). Almost all of these have projected separations of <15 AU, with the majority having separations of <7 AU. This tight binary distribution was initially viewed as evidence for the ejection scenario of brown dwarf formation (Close et al. 2003). In the ejection scenario, brown dwarfs are stellar embryos which are expelled from their natal subclusters due to interaction with other subcluster members, therefore cutting off accretion. Only tight brown dwarf binaries can survive an ejection event (Reipurth & Clarke 2001).

In the last decade, a population of wide (>15 AU separation) very low mass star, brown dwarf, and "planetary mass" ($<13\,M_{\rm Jup}$) binaries has been discovered in young (<12 Myr) nearby clusters (Luhman 2004; Chauvin et al. 2005; Kraus et al. 2005, 2006; Allers 2006; Jayawardhana & Ivanov 2006; Close et al. 2007; Konopacky et al. 2007; Todorov et al. 2010; Béjar et al. 2008, see Table 1 for a list of all young $\leqslant0.1\,M_\odot$ binaries). These recent results suggest that the multiplicity properties of young (∼few Myr) substellar objects in star-forming regions may be substantially different from the old (∼few Gyr) field population. If common, these young binaries also provide serious constraints for current theories of brown dwarf formation, since such wide binaries cannot be formed by a non-dissipative ejection model (Bate 2009). However, most of these objects were either discovered serendipitously, are from surveys with

unpublished statistics, or are from surveys with very few objects of comparable mass, so it is unknown how significant a population they form. Here, we conduct a systematic survey to search for such binaries in Upper Sco, the nearest OB association to the Earth.

2. SAMPLE SELECTION

At an age of ∼5 Myr and a distance of 145 pc (Preibisch et al. 2002), the Upper Scorpius OB association is one of the nearest sites of ongoing star formation and is intermediate in age between very young star-forming regions such as Taurus (<1 Myr) and somewhat older young field objects (∼100 Myr). Additionally, Upper Sco is denser than nearby T associations such as Taurus and Chamaeleon but considerably less dense than high-mass star-forming regions such as the Trapezium in Orion (Preibisch & Mamajek 2008). Binarity of young objects may vary both as a function of age and environment (Preibisch & Mamajek 2008). Certainly, the existence of very young, wide binaries in <2 Myr star-forming regions (e.g., Luhman 2004; Allers 2006; Jayawardhana & Ivanov 2006; Close et al. 2007; Konopacky et al. 2007; Todorov et al. 2010) and the absence of such binaries in the field population (e.g., Close et al. 2003) suggest that some evolution of brown dwarf binary properties must occur as a function of age. Thus, Upper Sco provides a key binary data point, intermediate in both age and density.

Some low-mass stars and high-mass brown dwarfs in Upper Sco have already been studied for binarity (Kraus et al. 2005, 2008). Numerous binarity studies have been conducted which are sensitive to very low substellar mass companions for very young clusters such as Taurus (Kraus et al. 2006; Konopacky et al. 2007), Chamaeleon (Ahmic et al. 2007), IC 348 (Luhman et al. 2005), NGC 1333 (Greissl et al. 2007), as well as

---

Table 1
Known Young (<15 Myr) Very Low Mass Binaries (Primary Mass $\lesssim 0.1\,M_\odot$)

ID	R.A.	Decl.	SpT1	SpT2	Mass1	Mass2	Proj. Sep. ($''$)	Proj. Sep. (AU)	Ref. Notes
Orion (400 pc, <1 Myr)									
2MASS J05352184−0546085	05:35:21.84	−05:46:08.5	M6.5	M6.5	$55\,M_{\rm Jup}$	$35\,M_{\rm Jup}$	$\cdots$	0.04 AU	a, b
Taurus (140 pc, <1 Myr)									
V410-Xray3	04:15:01.9[c]	28:18:48.[c]	M6	M7.7	$0.093\,M_\odot$	$0.047\,M_\odot$	$0.044 \pm 0\farcs002$	∼6 AU	d, e
MHO-Tau-8	04:33:01.1	24:21:11.0	M6	M6.6	$0.097\,M_\odot$	$0.073\,M_\odot$	$0.044 \pm 0\farcs008$	∼6 AU	d, f
2MASS J04414489+2301513AB	04:41:44.89	23:01:51.3	M8.5	$\cdots$	$\sim20\,M_{\rm Jup}$	5–$10\,M_{\rm Jup}$	$1\farcs105$	15 AU	g
CFHT-Tau 18	04:29:21.65	27:01:25.95	M6.0	$\cdots$	$0.1\,M_\odot$	$0.06\,M_\odot$	$0.216 \pm 0\farcs002$	30.2 AU	h, i
CFHT-Tau 7	04:32:17.86	24:22:14.98	M6.5	$\cdots$	$0.07\,M_\odot$	$0.06\,M_\odot$	$0.224 \pm 0\farcs002$	31.4 AU	h, i
CFHT-Tau 17	04:40:01.74	25:56:29.23	M5.75	$\cdots$	$0.1\,M_\odot$	$0.06\,M_\odot$	$0.575 \pm 0\farcs002$	80.5 AU	h, i
FU Tau AB	04:23:35.39	25:03:03.05	M7.25	M9.25	$\sim0.05\,M_\odot$	$\sim0.015\,M_\odot$	$5\farcs7$	800 AU	j
Ophiuchus (125 pc, <1 Myr)									
Oph 16AB	16:23:36.09	−24:02:20.9	$M5 \pm 3$	$M5.5 \pm 3$	$\sim100\,M_{\rm Jup}$	$\sim73\,M_{\rm Jup}$	$1\farcs7$	212 ± 43 AU	k, l
Oph 11AB	16:22:25.21	−24:05:13.94	$M9 \pm 0.5$	$M9.5 \pm 0.5$	$17^{+4}_{-5}\,M_{\rm Jup}$	14^{+6}_{-5}	$1\farcs9$	243 ± 55 AU	k, l, m, n
LkHα233 Group (325^{+72}_{-50} pc, ∼1 Myr)									
2MASS J22344161+4041387	22:34:41.61	40:41:38.7	M6	M6	$\sim0.1\,M_\odot$	$\sim0.1\,M_\odot$	$0\farcs16$	51 AU	o
Chamaeleon (160 pc, <3 Myr)									
Cha Hα 8	11:07:47.8	−77:40:08	M6.5	$\cdots$	0.07 - $0.1\,M_\odot$	30–$35\,M_{\rm Jup}$	$\cdots$	1 AU	p, q, r
2MASS J11011926−7732383AB	11:01:19.22	77:32:38.60	$M7.25 \pm 0.25$	$M8.25 \pm 0.25$	$0.05\,M_\odot$	$0.025\,M_\odot$	$1\farcs44$	240 AU	s
Upper Sco (145 pc, ∼5 Myr)									
USco-109AB	16:01:19.10	−23:06:38.6	M6	M7.5	$0.07\,M_\odot$	$0.04\,M_\odot$	$0.034 \pm 0\farcs02$	∼5 AU	t, u
USco-66AB	16:01:49.66	−23:51:07.4	M6.0	M6.0	$0.07 \pm 0.02\,M_\odot$	$0.07 \pm 0.02\,M_\odot$	$0\farcs07$	10.19 ± 0.07 AU	t, u
USco-55AB	16:02:45.60	−23:04:49.8	M5.5	M6.0	$0.10 \pm 0.03\,M_\odot$	$0.07 \pm 0.02\,M_\odot$	$0\farcs12$	17.63 ± 0.09 AU	t, u
UScoCTIO108AB	16:05:53.94	−18:18:42.7	M7	M9.5	$60 \pm 20\,M_{\rm Jup}$	$14^{+2}_{-8}\,M_{\rm Jup}$	$4.6 \pm 0\farcs1$	∼670	u, v
R Corona Australis (∼130 pc, ∼0.5–10 Myr)									
DENIS-P J185950.9−370632	18:59:50.9	−37:06:32	$M8 \pm 0.5$	$\cdots$	$0.017\,M_\odot$	$0.013\,M_\odot$	$0\farcs06$	7.8 AU	w
TW Hydra (∼30–70 pc, ∼12 Myr)									
2MASS J1207334393254	12:07:33.40	39:32:54.0	M8	L5-L9.5	$\sim25\,M_{\rm Jup}$	$5 \pm 2\,M_{\rm Jup}$	$0\farcs78$	55 AU	x, y

References. (a) Stassun et al. 2006; (b) Stassun et al. 2007; (c) Epoch 1950 coordinates; (d) Kraus et al. 2006; (e) Strom & Strom 1994; (f) Briceño et al. 1998; (g) Todorov et al. 2010; (h) Konopacky et al. 2007; (i) Guieu et al. 2006; (j) Luhman et al. 2009; (k) Allers 2006; (l) Close et al. 2007; (m) Jayawardhana & Ivanov 2006; (n) estimated age ∼5 Myr; (o) Allers et al. 2009; (p) Joergens 2006; (q) Joergens & Müller 2007; (r) Joergens et al. 2010; (s) Luhman 2004; (t) Kraus et al. 2005; (u) Ardila et al. 2000; (v) Béjar et al. 2008; (w) Bouy et al. 2004; (x) Chauvin et al. 2005; (y) Mohanty et al. 2007.

Table 2
Objects Observed

ID	R.A.	Decl.	SpT	J	H	K	$\mu_\alpha \cos \delta$[a]	μ_δ[a]
Objects from Lodieu et al. (2008) sample								
USco J155419.99−213543.1	15:54:19.99	−21:35:43.1	M8	14.93	14.28	13.71	−14	−18
USco J160603.75−221930.0	16:06:03.75	−22:19:30.0	L2	15.85	15.10	14.44	⋯	⋯
USco J160606.29−233513.3	16:06:06.29	−23:35:13.3	L0	16.20	15.54	14.97	⋯	−4
USco J160714.79−232101.2	16:07:14.79	−23:21:01.2	L0	16.56	15.83	15.07	⋯	−4
USco J160723.82−221102.0	16:07:23.82	−22:11:02.0	L1	15.20	14.56	14.01	−11	−31
USco J160727.82−223904.0	16:07:27.82	−22:39:04.0	L1	16.81	16.09	15.39	⋯	⋯
USco J160737.99−224247.0	16:07:37.99	−22:42:47.0	L0	16.76	16.00	15.33	⋯	⋯
USco J160818.43−223225.0	16:08:18.43	−22:32:25.0	L0	16.01	15.44	14.70	⋯	⋯
USco J160828.47−231510.4	16:08:28.47	−23:15:10.4	L1	15.45	14.78	14.16	−12	−13
USco J160830.49−233511.0	16:08:30.49	−23:35:11.0	M9	14.88	14.29	13.76	−5	−12
USco J160843.44−224516.0	16:08:43.44	−22:45:16.0	L1	18.58	17.22	16.26	⋯	−12
USco J160847.44−223547.9	16:08:47.44	−22:35:47.9	M9	15.69	15.09	14.53	0	−20
USco J160918.69−222923.7	16:09:18.69	−22:29:23.7	L1	18.08	17.06	16.16	⋯	−8
USco J161047.13−223949.4	16:10:47.13	−22:39:49.4	M9	15.26	14.57	14.01	−15	−24
USco J161228.95−215936.1	16:12:28.95	−21:59:36.1	L1	16.41	15.56	14.79	⋯	⋯
USco J161302.32−212428.4	16:13:02.32	−21:24:28.4	L0	17.17	16.37	15.65	⋯	⋯
USco J161441.68−235105.9	16:14:41.68	−23:51:05.9	L1	16.07	15.34	14.62	⋯	⋯
USco J163919.15−253409.9	16:39:19.15	−25:34:09.9	L1	17.20	16.39	15.61	−1	−17
Additional objects								
SCH J16091837−20073523	16:09:18.37	−20:07:35.23	M7.5	13.00	12.37	12.01	⋯	⋯
SCH J16224384−19510575	16:22:43.84	−19:51:05.75	M8	12.35	11.61	11.15	⋯	⋯

Note. [a] Lodieu et al. (2007).

Upper Sco (Kraus et al. 2005)—however, the least massive primaries observed in these surveys have generally been limited to higher mass brown dwarfs ($>40 M_{\rm Jup}$). To date, only 18 objects with estimated masses $<40 M_{\rm Jup}$ possess AO or space-based observations for binarity which are published in surveys with well-defined contrast limits (7 objects from Kraus et al. 2005 and 11 objects from Luhman et al. 2005).

Here, we extend binarity results to lower mass brown dwarfs and planetary mass objects in Upper Sco. We surveyed a sample of 20 substellar objects in Upper Sco with reported spectral types of M7.5 or later. These objects were selected from those with spectroscopic confirmation (Lodieu et al. 2008) from the near-IR photometric and proper motion surveys of Lodieu et al. (2007) and Slesnick et al. (2008). According to the models of Baraffe et al. (2003), these objects are all substellar. Indeed, these are the least massive objects currently known in Upper Sco, with estimated masses of $<40 M_{\rm Jup}$, thus this survey doubles the number of young, low-mass brown dwarfs imaged to search for binarity. At the 5 Myr age of Upper Sco, these objects are quite hot, hence their late-M and early-L spectral types. Eventually, these objects will cool to become T dwarfs. We focus in particular on 18 objects selected from Lodieu et al. (2008) which form a consistently selected and analyzed sample. Survey objects are listed in Table 2.

3. OBSERVATIONS AND DATA REDUCTION

We observed 20 objects with the facility infrared camera NIRC2 and the Laser Guide Star adaptive optics system (LGS AO; Bouy et al. 2004; Wizinowich et al. 2004) on the 10 m Keck II telescope. Observations were conducted on the nights of 2007 July 17, 2008 July 27, 2009 May 29, 2009 May 30, and 2009 June 30. Conditions varied considerably between nights. We used the NIRC2 narrow camera, with a 9.963 ± 0.005 mas pixel^{-1} platescale and a $10''.2 \times 10''.2$ field of view. Search observations were conducted in the Ks filter ($\lambda_{\rm central}$ =

2.146 μm). Objects were observed using a three-point dither pattern, with a dither of $1''-2''.5$ between positions. Observations are detailed in Table 3. The data were reduced in real time at the telescope using a custom IRAF pipeline. In cases where a candidate companion was detected at the telescope, immediate follow-up observations in J and H bands were then conducted. The observed object FWHM (K_S band) varied from 55 to 130 mas, with Strehl ratios in K_S varying from 6% to 29%. FWHMs and Strehl ratios were calculated using the standard Keck LGS routine nirc2strehl.pro. Most objects appeared slightly elongated in the direction of the tip-tilt reference star. We used a custom IDL pipeline for a final reduction of the data. The IDL pipeline corrects for on-chip distortion, flat fields, sky subtracts, and registers images using a cross-correlation algorithm.

4. CANDIDATE SELECTION TECHNIQUE AND TENTATIVE COMPANION CANDIDATES

Images were visually inspected for candidate companions. A number of faint candidate companions to several survey objects were identified at separations of $>1''$. To be considered true companions, candidates must possess red colors similar to their primary and have common proper motion. Candidates to USco J160603.75−221930.0 and USco J160723.82−221102.0 were reobserved one year after the initial observations and found to be background (i.e., not common proper motion objects). Colors for other candidates were checked in the $ZYJHK$ bands of the UK Infrared Deep Sky Survey (UKIDSS) or in the Digital Sky Survey (DSS). The UKIDSS project is defined in Lawrence et al. (2007). UKIDSS uses the UKIRT Wide Field Camera (WFCAM; Casali et al. 2007). The photometric system is described in Hewett et al. (2006), and the calibration is described in Hodgkin et al. (2009). The pipeline processing and science archive are described in M. J. Irwin et al. (2011, in preparation) and Hambly et al. (2008). One candidate companion to USco J160830.49−233511.0 was too faint to be detected in the

Table 3
Observations

ID	Observation Date	Filter	Exposure Time	Median Strehl	Median FWHM
Objects from Lodieu et al. (2008) sample					
USco J155419.99−213543.1	2009 May 30	K_S	7 × 60 s	0.10	99 mas
USco J160603.75−221930.0	2007 Jul 17	K_S	11 × 15 s	0.19	66 mas
		J	9 × 30 s	0.03	66 mas
		H	9 × 15 s	0.06	57 mas
	2008 Jul 27	K_S	11 × 15 s	0.31	55 mas
USco J160606.29−233513.3	2009 May 29	K_S	6 × 60 s	0.15	81 mas
USco J160714.79−232101.2	2009 May 29	K_S	6 × 60 s	0.10	80 mas
		J	6 × 60 s	0.02	95 mas
		H	6 × 60 s	0.05	92 mas
USco J160723.82−221102.0	2008 Jul 27	K_S	14 × 15 s	0.25	67 mas
		J	12 × 30 s	0.03	82 mas
		H	12 × 15 s	0.11	66 mas
	2009 May 30	K_S	7 × 60 s	0.13	82 mas
USco J160727.82−223904.0	2008 Jul 27	K_S	11 × 15 s	0.21	62 mas
		J	9 × 30 s	0.02	74 mas
USco J160737.99−224247.0	2009 May 29	K_S	6 × 60 s	0.11	96 mas
USco J160818.43−223225.0	2009 May 29	K_S	6 × 60 s	0.24	66 mas
USco J160828.47−231510.4	2007 Jul 17	K_S	11 × 15 s	0.13	82 mas
USco J160830.49−233511.0	2009 May 30	K_S	7 × 60 s	0.06	130 mas
USco J160843.44−224516.0	2009 May 29	K_S	6 × 60 s	0.16	78 mas
		J	6 × 60 s	0.02	70 mas
USco J160847.44−223547.9	2007 Jul 17	K_S	11 × 15 s	0.23	68 mas
USco J160918.69−222923.7	2008 Jul 27	K_S	11 × 15 s	0.13	67 mas
USco J161047.13−223949.4	2007 Jul 17	K_S	11 × 15 s	0.19	73 mas
USco J161228.95−215936.1	2008 Jul 27	K_S	11 × 15 s	0.16	67 mas
USco J161302.32−212428.4	2009 May 30	K_S	7 × 60 s	0.16	79 mas
USco J161441.68−235105.9	2008 Jul 27	K_S	11 × 15 s	0.16	67 mas
USco J163919.15−253409.9	2008 Jul 27	K_S	11 × 15 s	0.19	62 mas
		J	9 × 30 s	0.02	69 mas
Additional objects					
SCH J16091837−20073523	2009 Jun 30	K_S	6 × 20 s	0.11	75 mas
		J	6 × 20 s	0.01	80 mas
		H	6 × 20 s	0.04	71 mas
SCH J16224384−19510575	2009 May 30	K_S	6 × 10 s	0.29	59 mas

UKIDSS data ($K_s \sim 19$). This candidate will be reobserved at Keck in Spring 2011; however, given its faintness and wide separation ($\sim 5\rlap{.}''4$, ~ 780 AU), it is most likely background. All of the other $>1''$ candidates were detected with S/N > 10 in our Keck LGS AO data and were well detected in the UKIDSS data. All UKIDSS detected objects were found to have colors significantly bluer than their primary; this is a clear sign that these objects are blue background objects as opposed to a red brown dwarf or planetary mass companion.

Since our survey objects are quite faint and our AO correction is in general moderate, we did not attempt point-spread function (PSF) subtraction to search for faint companions within $1''$ of the object. Most of our objects show some elongation toward the tip-tilt star. Additionally, image quality varied considerably between nights and during individual nights. Thus, it was not possible to build a reliable synthetic PSF for PSF subtraction. We note that our brighter targets had a number of superspeckles evident within $0\rlap{.}''5$ of the primary which can mimic the appearance of a companion. However, these superspeck-

les modulate with wavelength and also evolve as a function of time. By comparing multiple images taken at different times or wavelengths, it is almost always possible to distinguish speckles from real companions. In fact, we did initially flag a number of close-in candidates which proved to be speckles upon further examination.

5. DISCOVERY OF A BROWN DWARF COMPANION TO SCH 16091837−20073523

A close candidate companion ($0\rlap{.}''14$) was detected around SCH J16091837−20073523 (henceforth SCH 1609-2009) with colors consistent with a young substellar object. JHK_S images of the companion and primary are presented in Figure 1. Photometry and astrometry for this object are presented in Table 4. Photometry and astrometry were determined using two different methods: (1) DAOPHOT PSF-fitting photometry using IRAF and (2) synthetic PSF-building photometry using BINFIT and StarFinder in IDL.

Table 4
Properties of the SCH1609-2007AB System

Property	Primary	Secondary
Distance	145 ± 2 pc[a]	
Age	5 Myr[b]	
Separation	0.144 ± 0″002 (20.9 ± 0.4 AU)	
Position angle	15.87 ± 0°13	
ΔJ (mag)	⋯	0.51 ± 0.09
ΔH (mag)	⋯	0.51 ± 0.03
ΔK_S (mag)	⋯	0.46 ± 0.01
J (mag)	13.53 ± 0.09[c]	14.04 ± 0.09
H (mag)	12.90 ± 0.04[c]	13.41 ± 0.04
K_S (mag)	12.56 ± 0.03[c]	13.01 ± 0.03
$J - K_S$ (mag)	0.97 ± 0.09	1.03 ± 0.09
$J - H$ (mag)	0.63 ± 0.10	0.63 ± 0.10
$H - K_S$ (mag)	0.34 ± 0.05	0.40 ± 0.05
Log $\frac{L}{L_\odot}$	−2.04 ± 0.12	−2.23 ± 0.12
Spectral type	M7 ± 0.5	M6 ± 1.0
$T_{\rm eff}$	2990 ± 60 K	2850 ± 170 K
Estimated mass (5 Myr)	79 ± 17 $M_{\rm Jup}$	55 ± 25 $M_{\rm Jup}$
Estimated mass (10 Myr)	84 ± 15 $M_{\rm Jup}$	60 ± 25 $M_{\rm Jup}$

Notes.
[a] Preibisch et al. (2002).
[b] Preibisch & Zinnecker (1999).
[c] From 2MASS.

For the DAOPHOT PSF-fitting photometry, a background object in the field (with separation $>5''$ from the primary and blue colors as expected for a background object) was used as a PSF for the allstar task. The PSF object was well detected in both H and K bands. However, our reduced AO correction in the blue J band relative to the H and K resulted in a lower signal-to-noise detection of the PSF star in the J band, diminishing our photometric accuracy in the J band.

Since we were somewhat concerned that the background object used as a PSF at $>5''$ might be affected by anisoplanetism, we also determined the binary separation, position angle (P.A.), and flux ratio using the StarFinder PSF-fitting software package (Diolaiti et al. 2000) as an independent confirmation of the DAOPHOT results. StarFinder simultaneously solves for an empirical PSF model and the positions and fluxes of the binary components. Our J-band images had significantly poorer FWHMs and Strehl ratios such that StarFinder did not converge on a solution. Thus, for the J band we instead used a three-component Gaussian model, as described by Dupuy et al. (2009), to derive the binary parameters from PSF fitting. The uncertainties were determined from the rms of the best-fit parameters for our individual dithered images. We adopted the astrometric calibration of Ghez et al. (2008), with a pixel scale of 9.963 ± 0.005 mas pixel^{-1} and an orientation for the detector's $+y$-axis of $+0°13 ± 0°02$ east of north. We applied the distortion correction developed by B. Cameron (2007, private communication), which changed our astrometry below the 1σ level. Both DAOPHOT and StarFinder methods yielded nearly identical values (within the cited errors) for photometry and astrometry.

We show the primary and companion on color–magnitude and color–color diagrams in Figure 2. The companion possesses very similar colors to its primary, suggesting that it is a true substellar companion. We estimated the likelihood that this companion is a background object using source counts from the 2MASS survey. Within 1° of the primary, 2MASS detects 527 objects with J of 13 mag or brighter, 506 objects with H
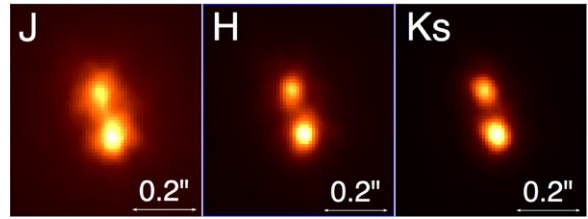

Figure 1. Left: J-, H-, and K_S-band images of SCH 16091837-20073523AB obtained with NIRC2 and the LGS AO system of the 10 m Keck II telescope. North is up and east is left. Note that primary and companion both appear slightly elongated in the direction toward the tip-tilt star. The confirmed companion is at 0″144 ± 0°13 separation and P.A. = 15.87 ± 0°13 with flux ratios of $\Delta J = 0.51 ± 0.09$, $\Delta H = 0.51 ± 0.03$, and $\Delta K_S = 0.46 ± 0.01$ mag. We estimate masses of 79 ± 17 $M_{\rm Jup}$ and 55 ± 25 $M_{\rm Jup}$ for primary and companion respectively (5 Myr age).

(A color version of this figure is available in the online journal.)

of 12.4 or brighter, and 427 with K of 12 or brighter. Thus, adopting the approach of Brandner et al. (2000), in particular, their Equation (1), we estimate the probability of finding an unrelated source at least as bright as the observed companion within 0″14 of the primary to be $\sim 2.6 \times 10^{-6}$.

SCH 1609-2007 was reobserved with NIRC2 at Keck II on 2010 May 1. The overall quality of the data set was poor; however, we acquired sufficient data to demonstrate that the companion likely has common proper motion with the primary. Measuring centroid positions of the primary and companion (as the second epoch data were not high enough quality for PSF-fitting photometry), the companion moved by <0.7 pixels relative to the primary between epochs, consistent with the errors in our simple center-of-light centroiding. As no directly measured proper motion is available for SCH 1609-2007 we adopt the mean value of $(-11, -25)$ mas yr^{-1} for Upper Sco here (de Bruijne et al. 1997; Preibisch et al. 1998). At a distance of 145 pc, parallax motion for Upper Sco is quite small: ~ 7 mas. As the parallax factor in the second epoch observation was similar to that in the first, we neglect parallax here. With the ~ 10 mas pixel scale of the narrow camera, we would have expected the companion to move ~ 2.3 pixels relative to the primary between epochs if it was a background object at a much larger distance. Thus, this is likely a proper motion pair.

5.1. Spectroscopy and Spectral Type Estimates

It has been noted that objects from Slesnick et al. (2008) are considerably brighter than objects of similar spectral type from Lodieu et al. (2008). In fact, in some cases, the discrepancy is as much as 2 or 3 mag, e.g., the M8 objects SCH J1622−1951 and USco J155419.99−213543.1 in the sample for this survey. One possible explanation for this discrepancy is that the later type Slesnick et al. (2008) objects consist primarily of nearly equal mass binaries, such as SCH J1609 and likely SCH 1622-1951 as well. However, even after accounting for binarity, SCH J1609−2007 is still 2–3 mag overluminous compared to similar objects from the Lodieu et al. (2008) sample.

The discrepancy may also be due to systematic differences between optical and infrared spectral types for these objects, which are right at the M to L type spectral transition. All of the Slesnick et al. (2008) sources have optical spectral types while the Lodieu et al. (2008) sources have infrared ones, so in effect we may be comparing apples versus oranges. Thus, to further constrain the near-IR spectral type (and hence mass) of SCH J1609−2007AB we obtained integrated-light near-IR spectroscopy of SCH1609-2007 on 2010 September 14 (UT)
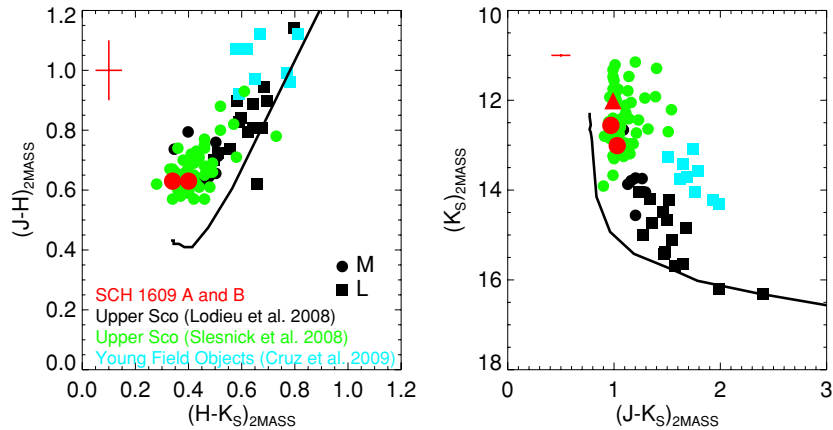
Figure 2. Left: the JHK_S colors of SCH 1609 AB compared to Upper Sco objects with M and L spectral types (Slesnick et al. 2008; Lodieu et al. 2008) and young field brown dwarfs from Cruz et al. (2009). SCH 1609ABs' colors are plotted as a red circles and are consistent with those of a mid- to late-M dwarf. Errors on SCH 1609AB photometry are shown in the top left corner. The DUSTY 5 Myr isochrone is plotted as a solid line. DUSTY models predict considerably bluer colors at these ages than is observed. Right: $J-K_S$ vs. K_S for SCH 1609AB and the same set of comparison objects. SCH 1609AB is plotted as red circles; combined photometry for the system is plotted as a red triangle. The DUSTY 5 Myr isochrone is again plotted as a solid line; while K_S-band magnitudes agree with DUSTY predictions, colors are considerably redder than the predictions for M dwarfs.

(A color version of this figure is available in the online journal.)
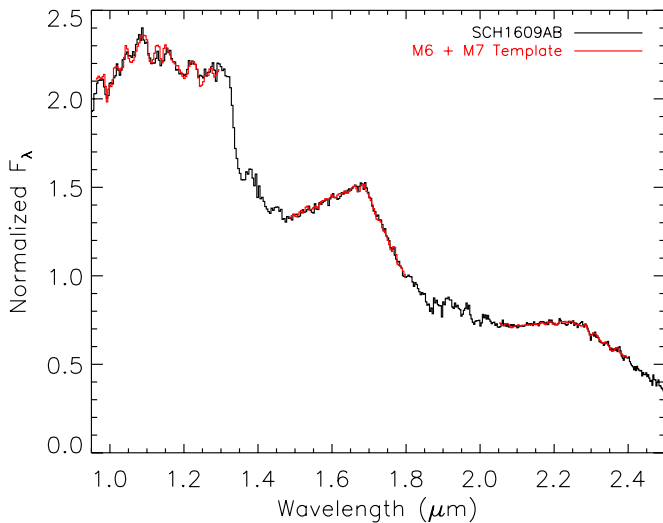
Figure 3. Composite near-IR spectrum of SCH1609AB (black), compared to the best-fitting synthetic composite spectrum (red). The synthetic composite spectrum is the combination of UScoCTIO 75 (M6; Ardila et al. 2000; Preibisch et al. 2002) and DENIS-P J155605.0−210646 (M7; Martin et al. 2004; Slesnick et al. 2008).

(A color version of this figure is available in the online journal.)

using the SpeX spectrograph (Rayner et al. 2003) on the NASA Infrared Telescope Facility. A series of 12 exposures of 30 s each were taken, nodding along the slit, for a total integration time of 6 minutes. Our observations were taken at an airmass of 1.57, and the seeing recorded by the IRTF was 0".9. The data were taken using the Low-Res prism with the 0".5 slit aligned with the parallactic angle, producing a 0.8–2.5 μm spectrum with a resolution ($R = \lambda/\Delta\lambda$) of ~150. For telluric correction of our SCH1609-2007 spectrum, we observed a nearby A0V star, HD 149827, and obtained calibration frames (flats and arcs). The spectra were reduced using the facility reduction pipeline, Spextool (Cushing et al. 2004), which includes a correction for telluric absorption following the method described in Vacca et al. (2003). Spectra and spectral fits are presented in Figure 3.

SCH1609-2007AB was assigned a composite optical spectral type of M7.5 by Slesnick et al. (2008). We determine spectral types for each component by comparing our integrated-light near-IR spectrum of SCH1609-2007AB to synthetic composites generated from template near-IR spectra of known members of Upper Scorpius (also taken with SpeX at the IRTF, at the same resolution as the SCH1609-2007AB spectrum; B. Bowler 2010, private communication). Our Upper Scorpius templates have optical spectral types ranging from M4 to M8.5. We verified that our templates have near-IR spectral types (calculated using the H_2O index of Allers et al. 2007) that agree to within one subtype with their optical types.

To create our synthetic composite spectra, we first calculated synthetic photometry for each template using the J, H, and K_S filter profiles for NIRC2 and normalized each spectrum by the photometric flux density. We interpolated the templates to the same wavelength grid as our spectrum of SCH1609-2007, and summed pairs of template spectra together, multiplying the later spectral type template by the flux ratio of the binary. Following the technique described in Cushing et al. (2008), we determined a multiplicative constant for each template in each band (J, H, and K_S), and computed a reduced χ^2 performed over the wavelength ranges $\lambda = 0.96$–1.3 μm, 1.48–1.8 μm, and 2.05–2.4 μm. The best-fitting template is the composite spectrum of UScoCTIO 75 (M6; Ardila et al. 2000; Preibisch et al. 2002) and DENIS-P J155605.0−210646 (M7; Martín et al. 2004, Slesnick et al. 2008). We assign spectral types of M6.0 ± 0.5 to SCH1609-2007A and M7.0 ±1.0 to SCH1609-2007B, where uncertainties are determined from the spectral types of synthetic composite spectra where $\chi^2 \geqslant \chi^2_{min}$ + 1, significantly earlier than the combined M7.5 spectral type from Slesnick et al. (2008).

5.2. Mass Estimates

We estimate the masses and effective temperatures of SCH 1609-2007 AB based on the DUSTY models of Chabrier et al. (2000) and the temperature scale of Luhman (2004). The age of Upper Scorpius has been measured as 5 Myr, with a spread of up to 2 (Preibisch & Zinnecker 1999; Slesnick et al. 2008),
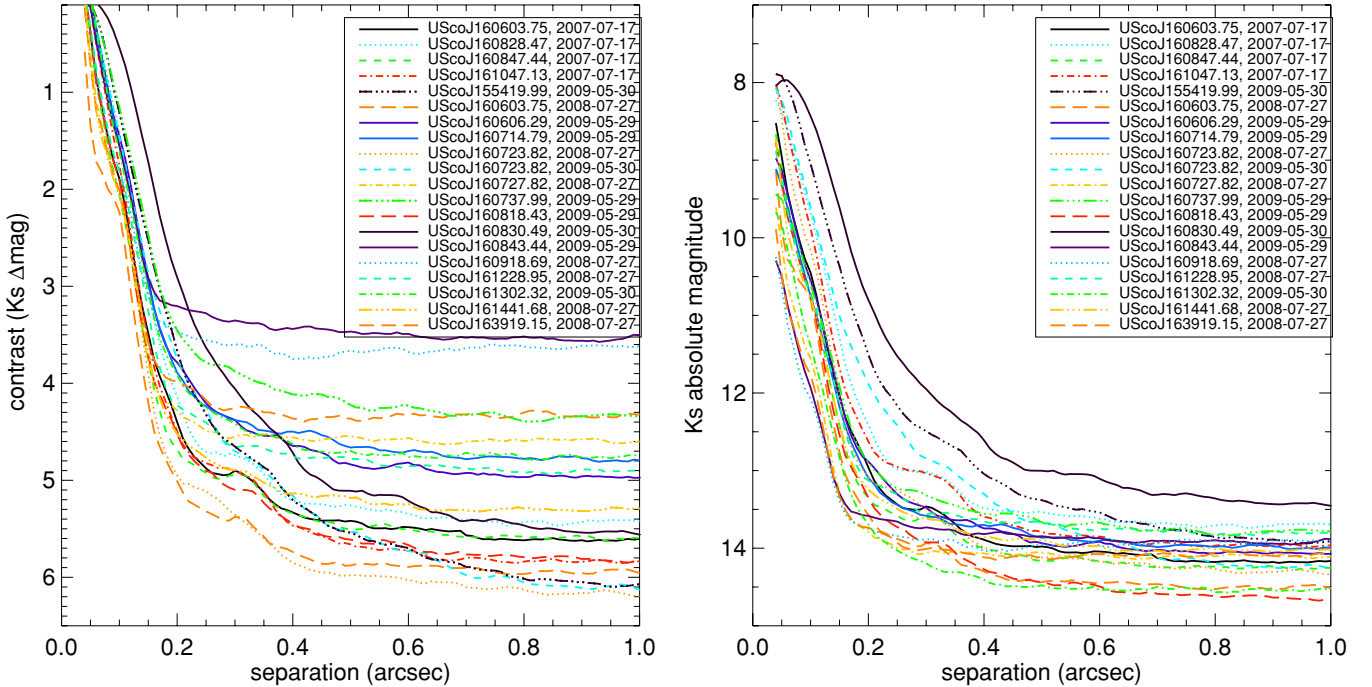
Figure 4. Left: 5σ contrast curves for 18 survey objects from Lodieu et al. (2008). Noise levels after data reduction were calculated as a function of radius by calculating the standard deviation in an annulus (with width equal to approximately the FWHM of the PSF) centered on that radius. Noise curves were then converted to contrast in Δmag by dividing by the measured peak pixel value of the object. In general, we achieve contrasts of >4 mag at separations of $\geqslant 0\farcs4$, sufficient to detect a 2MASS 1207 analogue at the distance of Upper Sco. Right: minimum detectable absolute magnitude for the same 18 objects. Contrasts were converted into absolute magnitudes using photometry reported in Lodieu et al. (2008) and Slesnick et al. (2008), and adopting a distance of 145 pc for Upper Sco. A filter transform was calculated from K to K_s band using the spectra from Lodieu et al. (2008).

(A color version of this figure is available in the online journal.)

but more recent work suggests ages as old as 10 Myr (E. E. Mamajek 2010, private communication).

Thus to account for age spread, we estimate masses at discrete ages of 5 and 10 Myr using the DUSTY models (Chabrier et al. 2000) and at an age range of 5 ± 1 Myr using dust-free models from the same group (Baraffe et al. 1998, 2002).[7] For single age mass estimates, we simulated the spectral type range of each object with an input distribution of 10^6 Gaussian-distributed spectral type values centered on the measured spectral type and with σ set to the error on the measured spectral type. We then converted this input distribution to effective temperatures using the temperature scale of Luhman (2004) and to estimated mass using the Chabrier et al. (2000) models. The estimated mass of each object was set to the mean of the output distribution and the error on the mass was set to the standard deviation of the output distribution. Via this method, we estimate primary and secondary masses of $79 \pm 17\,M_{\rm Jup}$ and $55 \pm 25\,M_{\rm Jup}$ at an age of 5 Myr and masses of $84 \pm 15\,M_{\rm Jup}$ and $60 \pm 25\,M_{\rm Jup}$ at an age of 10 Myr.

For mass estimates for a range of ages, we simulated input spectral type and ages with an input distribution of 3×10^4 Gaussian-distributed spectral type and age values. As before, the spectral type values were centered on the measured spectral type, with σ set to the error on the measured spectral type. The

center of the age distribution was set as 5 Myr, with $\sigma = 1$ Myr. Interpolation with the Luhman (2004) temperature scale and Baraffe et al. (1998, 2002) models was performed to convert from spectral type to estimated mass for the distribution. Since the output distribution is somewhat asymmetric, we adopt the median as the best mass estimate and again use the standard deviation to set the error. Via this method, we estimate primary and secondary masses of $79 \pm 21\,M_{\rm Jup}$ and $60 \pm 31\,M_{\rm Jup}$. Thus, for the range of ages that are realistic for this binary, the uncertainty in the measured spectral type dominates the mass estimate above and beyond any uncertainty in the age.

5.3. Orbital Period Estimates

We estimate the semimajor axis of SCH 1609-2007AB's orbit from its observed separation. Assuming a uniform eccentricity distribution between $0 < e < 1$ and random viewing angles, Dupuy & Liu (2010) compute a median correction factor between projected separation and semimajor axis of $1.10^{+0.91}_{-0.36}$ (68.3% confidence limits). Using this, we derive a semimajor axis of $23.0^{+19.0}_{-7.5}$ AU for SCH 1609AB based on the observed separation in 2009 June. These correspond to an orbital period estimate of 310^{+222}_{-211} yr, for an assumed total system mass of $134 \pm 30\,M_{\rm Jup}$.

6. ACHIEVED CONTRASTS AND LIMITS ON MINIMUM DETECTABLE COMPANION MASSES

The 5σ contrast curves for our core sample of 18 objects from Lodieu et al. (2008) are presented in Figure 4. Noise levels after data reduction were calculated as a function of radius by calculating the standard deviation in an annulus (with width equal to the FWHM of the PSF) centered on that radius. Noise

---

[7] While these two sets of models differ in colors due to different atmospheric compositions (dust grains or the lack thereof), they produce the same bolometric luminosities and effective temperatures as a function of age and mass (Baraffe et al. 2002). In particular, since isochrones are only defined at 1, 5, and 10 Myr for the DUSTY models as opposed to a much denser grid of isochrones for the Baraffe et al. (1998) models—and the authors suggest caution using isochrones with ages $\leqslant$1 Myr, we have chosen to interpolate from the Baraffe et al. (1998) models when deriving masses at a range of ages to avoid inaccuracies from interpolating from 1 Myr isochrones.

Table 5
Measured K_s Contrast and Minimum Detectable Mass Ratios

ID	Observation Date	Δmag($0\rlap{.}''07$)	$q(0\rlap{.}''07)$	Δmag($0\rlap{.}''2$)	$q(0\rlap{.}''2)$	Δmag($0\rlap{.}''5$)	$q(0\rlap{.}''5)$
USco J155419.99−213543.1	2009 May 30	0.41	0.87	3.67	0.24	5.54	0.11
USco J160603.75−221930.0	2008 Jul 27	1.83	0.46	5.01	0.13	5.88	0.08
USco J160603.75−221930.0	2007 Jul 17	1.17	0.59	4.40	0.16	5.42	0.10
USco J160606.29−233513.3	2009 May 29	0.65	0.71	3.79	0.20	4.84	0.13
USco J160714.79−232101.2	2009 May 29	0.70	0.71	3.89	0.19	4.66	0.14
USco J160723.82−221102.0	2008 Jul 27	1.23	0.64	4.95	0.14	5.98	0.08
USco J160723.82−221102.0	2009 May 30	0.62	0.80	3.74	0.23	5.53	0.11
USco J160727.82−223904.0	2008 Jul 27	1.36	0.54	4.28	0.16	4.55	0.14
USco J160737.99−224247.0	2009 May 29	0.42	0.86	3.45	0.23	4.22	0.16
USco J160818.43−223225.0	2009 May 29	1.16	0.58	4.53	0.15	5.61	0.08
USco J160828.47−231510.4	2007 Jul 17	0.59	0.80	4.14	0.19	5.26	0.12
USco J160830.49−233511.0	2009 May 30	0.14	0.95	2.91	0.32	5.11	0.13
USco J160843.44−224516.0	2009 May 29	0.78	0.72	3.20	0.27	3.47	0.23
USco J160847.44−223547.9	2007 Jul 17	1.23	0.56	4.68	0.14	5.51	0.10
USco J160918.69−222923.7	2008 Jul 27	1.11	0.63	3.46	0.23	3.66	0.21
USco J161047.13−223949.4	2007 Jul 17	0.82	0.75	4.49	0.17	5.66	0.10
USco J161228.95−215936.1	2008 Jul 27	1.08	0.60	4.23	0.17	4.78	0.13
USco J161302.32−212428.4	2009 May 30	0.69	0.76	3.91	0.18	4.70	0.11
USco J161441.68−235105.9	2008 Jul 27	1.48	0.52	4.52	0.15	5.18	0.11
USco J163919.15−253409.9	2008 Jul 27	1.38	0.56	3.98	0.18	4.36	0.14

curves were then converted to contrast in Δmag by dividing by the measured peak pixel value of the object. Contrasts were converted into absolute magnitudes using photometry reported in Lodieu et al. (2008) and adopting a distance of 145 pc for Upper Sco. A filter transform was calculated from K to K_s band using the spectra from Lodieu et al. (2008). Absolute magnitudes of the faintest detectable objects are also presented in Figure 4. A table of contrast values at separations of 0.07, 0.2, and $0\rlap{.}''5$ is presented in Table 5.

To test the fidelity of our contrast curves, we inserted and retrieved simulated objects in our data. Objects were simulated as two-dimensional Gaussians with FWHMs from fits to the primary using the IDL routine GAUSSFIT2D and contrasts from our measured contrast curves. Objects simulated with contrasts from our measured curves were retrieved with S/N $\geqslant$ 5 for all survey targets down to separations of $0\rlap{.}''07$. For separations down to $0\rlap{.}''06$, simulated objects were retrieved for half of our survey targets. No simulated objects were retrieved at separations $\leqslant 0\rlap{.}''05$. Thus, we conclude that our measured contrast curves are a reliable estimate of the detectable contrasts for potential companions down to separations of $0\rlap{.}''07$.

We note that these contrasts do not take into account confusion between potential companions and speckles. Our brighter targets had a number of superspeckles evident within $0\rlap{.}''5$ of the primary which can mimic the appearance of a companion. However, these superspeckles modulate with wavelength and also evolve as a function of time. By comparing multiple images taken at different times or wavelengths, it is almost always possible to distinguish speckles from real companions. Thus, since we can distinguish between the two, we believe that our contrast curves adequately measure obtained contrasts for this survey, despite potential speckle confusion.

Contrasts were converted to minimum detectable mass ratios using the models of Chabrier et al. (2000) at an adopted age of 5 Myr and assuming a similar bolometric correction (i.e., a similar spectral types for both objects) between each target and any potential companion (Figure 5 and Table 5). We note that for the best 75% of our data we are complete for all binaries with $q \geqslant 0.8$ at separations >10 AU and all binaries with $q \geqslant 0.2$ at separations >50 AU.
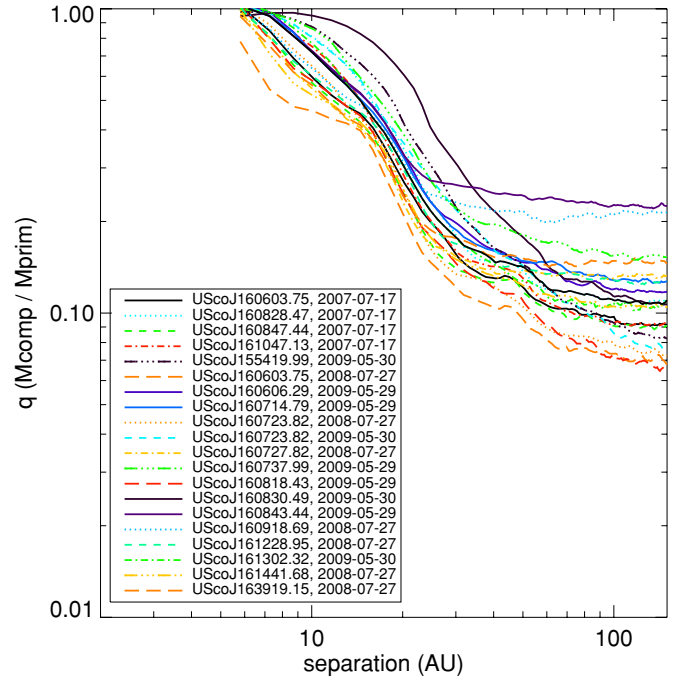

Figure 5. Mass ratio (q) vs. separation using the DUSTY models. Contrasts were converted to minimum detectable mass ratios using the models of Chabrier et al. (2000) at an adopted age of 5 Myr. For the best 75% of our data, we are complete to $q \sim 0.8$ at 10 AU and complete to $q \sim 0.2$ at $\geqslant$20 AU.

(A color version of this figure is available in the online journal.)

7. DISCUSSION

7.1. Measured Binary Fraction

We note that our newly discovered binary, SCH 1609AB, is consistent with other young, wide very low mass binaries discovered, with a wide (>10 AU) separation and nearly equal mass ratio ($q \sim 0.7$). With only one companion detected as part of our survey, we cannot place any new constraints on the mass ratio distribution or separation distribution for young brown dwarf companions. However, we have surveyed the largest

sample to date of young brown dwarfs with estimated masses $<40\,M_{\rm Jup}$ and can strengthen constraints on the binary fraction (10–500 AU) of young objects in this mass range. We find an upper limit on the binary fraction (10–500 AU) of 9% (1σ) for the 18 objects we surveyed from Lodieu et al. 2008 (calculated via the method of Burgasser et al. 2003). (We exclude the sources observed from the Slesnick et al. 2008 sample since they appear so much brighter than the Lodieu et al. sources and likely have masses $> 40\,M_{\rm Jup}$).

7.2. Methods for Statistical Comparisons between Samples

Given a sample of objects with true binary fraction $\epsilon_{\rm bin}$, the probability density of finding k binaries among n objects observed is given by the binomial distribution:

$$f(k; n, \epsilon_{\rm bin}) = \frac{n!}{k!(n-k)!}\epsilon_{\rm bin}^{k}(1-\epsilon_{\rm bin})^{n-k}. \quad (1)$$

In our case, we would like to invert this probability density in order to obtain the probability of the sample having a given binary fraction $\epsilon_{\rm bin}$ in the case that we measure k binaries among n objects. To estimate the true binary fraction for our sample, we can then derive a confidence interval (presented as $1-\sigma$ intervals here) around the maximum of this probability density in which we expect the true binary fraction to reside. The probability density function and the resulting confidence intervals can either be calculated numerically (via, e.g., the method of Burgasser et al. 2003) or by Bayesian posterior inference (see, e.g., Sivia & Skilling 2006 and Cameron 2010).

Quantitatively comparing the binary fractions (with error bars included from confidence intervals) from sample to sample requires some additional mathematical machinery. In some cases, the confidence intervals overlap for binary fractions derived for different samples—however, it is not immediately clear how statistically significant this correlation is. In comparing two samples of objects the question we wish to answer is: are they drawn from the same binomial distribution with $\epsilon_{\rm bin}$ or from different distributions? To determine the likelihood that two samples are drawn from the same binomial distribution, we adopted both the Fischer exact test method (used by Ahmic et al. 2007 and described in the Appendix of Brandeker et al. 2006) as well as a Bayesian approach, derived below (derivation adopted from Carpenter 2009).

According to Bayes' theorem:

$$\text{prob(hypothesis; data, I)} \propto \text{prob(data; hypothesis, I)}$$
$$\times \text{prob(hypothesis; I)}, \quad (2)$$

where (in this case) "I" is prior information, "data" is our measured sample, and "hypothesis" is the hypothesis (e.g., in this case we hypothesize that for brown dwarfs, phenomenon of binarity can be modeled as a binomial distribution with binary probability $\epsilon_{\rm bin}$). In Bayesian terms, prob(hypothesis; I) is the prior probability and represents what we initially know regarding the truth or falseness of the hypothesis while prob(data; hypothesis, I) is the likelihood function and gives the likelihood of each possible experimental outcome given the adopted model for the data. Combining the two gives prob(hypothesis; data, I), the posterior probability—the likelihood of a given model, in light of the measured data.

In this case, we would like to derive the posterior probability density not for each individual sample but for the difference of the two:

$$\delta = \epsilon_{\rm bin1} - \epsilon_{\rm bin2}. \quad (3)$$

To do this, we first must derive the posterior probability distributions appropriate for each of the two binomial distributions we are comparing. Our likelihood function is again given by the binomial distribution, where $\epsilon_{\rm bin}$ is the true binary fraction, for the sample, n is the total number of objects observed, and k is the number of binaries found:

$$\text{prob(data; hypothesis, I)} = f(k; n, p)$$
$$= \frac{n!}{k!(n-k)!}p^{k}(1-p)^{n-k}. \quad (4)$$

For the prior probability, prob(hypothesis; I), we simply adopt a uniform distribution from 0 to 1, i.e., the binary fraction must be between 0 and 1. This can also be written in terms of the Beta distribution, a special case of the Dirichlet distribution with only two parameters defined on the interval (0,1):

$$f(x; \alpha, \beta) = \frac{\Gamma(\alpha + \beta)}{\Gamma(\alpha)\Gamma(\beta)}x^{\alpha-1}(1-x)^{\beta-1}. \quad (5)$$

Adopting $\alpha = \beta = 1$, $f(x;1,1)$ reduces to a uniform distribution, thus:

$$\text{prob(hypothesis; I)} = 1\ \text{in the interval } 0, 1 = {\rm Beta}(1, 1). \quad (6)$$

The advantage of choosing the Beta distribution to represent the prior probability is that the Beta distribution is a conjugate distribution to the binomial distribution. In other words, if the prior probability is a Beta distribution and the likelihood is a binomial distribution, then the posterior probability will also be a Beta distribution. In this case, it is instructive to view the likelihood as an "operator" on the prior probability which produces as a result the posterior probability. When a binomial distribution "operates" on a Beta distribution with prior hyperparameters α and β, the result is the following posterior distribution:

$$\text{prob(hypothesis; data, I)} = {\rm Beta}(k + \alpha, n - k + \beta). \quad (7)$$

Thus, in our case where $\alpha = \beta = 1$:

$$\text{prob(hypothesis; data, I)} = {\rm Beta}(k + 1, n - k + 1). \quad (8)$$

Thus, our posterior probability distributions for each sample are given by

$$\text{prob}(\epsilon_{\rm bin1}; k_1, n_1) = {\rm Beta}(\epsilon_{\rm bin1}; k_1 + 1, n_1 - k_1 + 1) \quad (9)$$

$$\text{prob}(\epsilon_{\rm bin2}|k_2, n_2) = {\rm Beta}(\epsilon_{\rm bin2}|k_2 + 1, n_2 - k_2 + 1). \quad (10)$$

The posterior probability density for δ is then given by

$$\text{prob}(\delta; k, n) = \int_{-\infty}^{\infty} {\rm Beta}(\epsilon_{\rm bin}|k_1 + 1, n_1 - k_1 + 1)$$
$$\times {\rm Beta}(\epsilon_{\rm bin} - \delta|k_2 + 1, n_2 - k_2 + 1)\,d\epsilon_{\rm bin}. \quad (11)$$

We used Monte Carlo methods in the R programming language to evaluate this integral. 10^4 random deviates were taken from each posterior probability Beta distribution and the posterior probability density for δ was determined from these. Two representative posterior probability densities (for the case where both samples likely share the same binomial distribution and also the case where binomial distributions differ
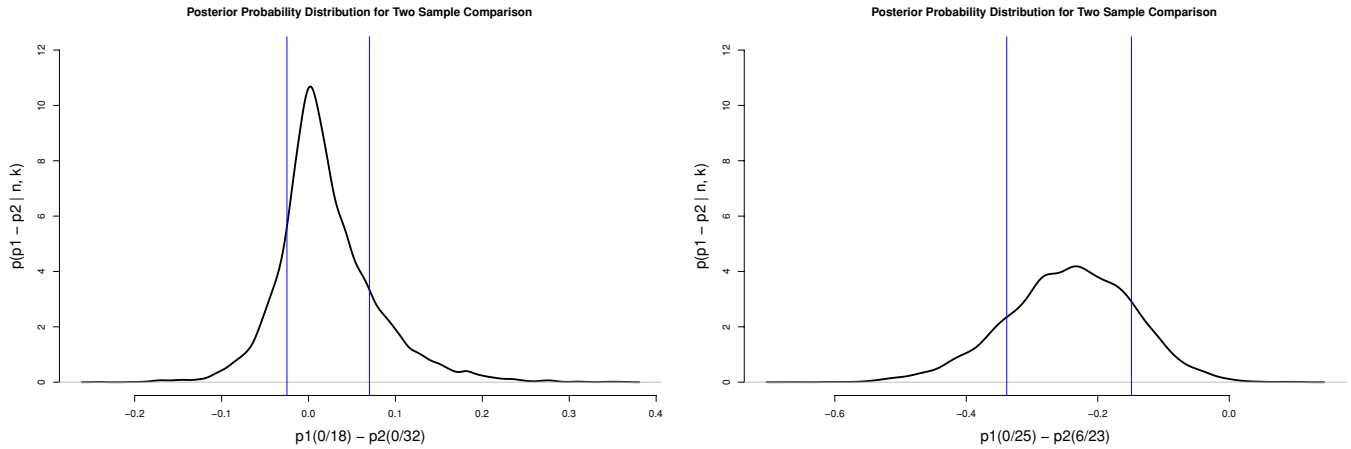
Figure 6. Sample posterior probability distributions. Blue lines show the 1σ confidence intervals on $\epsilon_{bin1} - \epsilon_{bin2} = p1 - p2$. Left: two samples which are likely drawn from the same binomial distribution (specifically $<0.04\ M_\odot$ BDs in Upper Sco with 0 binaries detected out of 18 objects, compared with field T dwarfs, with 0 binaries detected out of 32 objects). The posterior probability distribution is strongly peaked at 0 and shows little spread. Right: two samples which are likely drawn from different binomial distributions (specifically $<0.04\ M_\odot$ Upper Sco, Taurus, and Chamaeleon objects, with 0 binaries detected out of 25 objects, compared with 0.07–$0.1\ M_\odot$ Upper Sco, Taurus, and Chamaeleon objects, with 6 binaries detected out of 23 objects). The posterior probability distribution in this case peaks considerably away from 0, and is wider and flatter than the previous case. In particular, at the 1σ level $\epsilon_{bin2} = p2$ for the second distribution is between $\epsilon_{bin1} + 0.15$ and $\epsilon_{bin1} + 0.33$.

(A color version of this figure is available in the online journal.)

between samples) are presented in Figure 6. Here, we present the 1σ (68%) and 2σ (95%) confidence intervals from the posterior probability density for δ as a counterpart to the Fisher exact test likelihoods. These confidence intervals quantify the probable relationship between the true binary fractions of the two samples. For example, for the second comparison presented in Figure 6, a sample with 0 binary detected out of 25 objects compared with a sample of 6 binaries detected out of 23 objects at the 1σ level ϵ_{bin2} for the second distribution lies between $\epsilon_{bin1} + 0.15$ and $\epsilon_{bin1} + 0.33$.

7.3. Brown Dwarf Binary Fraction as a Function of Mass

We compare our measured binary fraction to that of more massive brown dwarfs and very low mass stars in the Upper Sco embedded cluster. Kraus et al. (2005) surveyed 12 brown dwarfs and very low mass stars with the ACS on the *HST*. These objects have estimated masses of 0.04–0.1 $M_\odot$ and thus comprise a higher mass sample than our survey. Kraus et al. (2005) discovered three binaries in this sample, one of which (USco-109 AB) is below the sensitivity of our survey to detect, with a projected separation of only ~5 AU. Thus, for the purposes of comparison, we adopt a binary fraction of $2/12 = 17^{+15}_{-6}$% for the Kraus et al. (2005) sample. The likelihood that the Kraus et al. (2005) sample is drawn from the same distribution as ours is 0.15, with a $1-\sigma$ Bayesian confidence interval of $\epsilon_{bin1} - \epsilon_{bin2} = -0.28, 0.15$. Thus, as noted by previous authors (Kraus et al. 2005), the binary fraction in Upper Sco continues to decrease with decreasing primary mass.

This comparison is limited by the relatively small number of objects observed in Upper Sco. Thus, to improve statistics, we have compiled a larger list using objects from similar surveys of other young, nearby regions—specifically Taurus (<1 Myr, 145 pc, objects from Kraus et al. 2006; Konopacky et al. 2007) and Chamaeleon (<3 Myr, 160 pc, objects from Ahmic et al. 2007). We include only companions that would have been detected at the sensitivity level of our survey and initially limit this analysis to nearby clusters (<200 pc) since more distant clusters (e.g., NGC 1333, IC 348, Serpens) are more than 250 pc distant and do not reach comparable sensitivity levels at 10 AU.

All selected surveys have similar sensitivity levels (complete to $q \sim 0.8$ at 10 AU, complete to $q \sim 0.2$–0.3 at $\geqslant 20$ AU) so it is unlikely that our survey would have discovered a binary at a separation >10 AU missed by these other surveys, and vice versa. We adopt three mass bins for this analysis: (1) high mass (0.07–$0.1\ M_\odot$), with 6 binaries detected out of 23 objects surveyed (6 objects from Ahmic et al. 2007, 5 from Kraus et al. 2006, 6 from Kraus et al. 2005, 4 from Konopacky et al. 2007, and the two objects from the Slesnick et al. 2008 sample from the current survey), (2) medium mass (0.04–$0.07\ M_\odot$), with 0 binaries detected out of 18 objects surveyed (4 objects from Ahmic et al. 2007, 6 from Kraus et al. 2005, and 8 from Kraus et al. 2006), and (3) low-mass ($<0.04\ M_\odot$), with 0 binaries detected out of 25 objects surveyed (7 objects from Kraus et al. 2006 and the 18 objects from the Lodieu et al. 2008 sample surveyed herein). We note that while a number of additional binaries are known in this mass range, e.g., 2MASS 1207AB (Chauvin et al. 2005), 2M 1622 (Allers 2006; Allers et al. 2006; Jayawardhana & Ivanov 2006; Allers et al. 2007; Close et al. 2007), UScoCTIO 108 (Béjar et al. 2008), and 2MASS 0441 (Todorov et al. 2010), survey statistics are not available for these objects and thus we cannot include them in our sample. Binary fractions and likelihoods between bins as a function of mass are presented in Table 6. As expected, the binary fraction decreases monotonically with primary mass. The likelihood that the low mass bin ($<0.04\ M_\odot$) objects share the same binary fraction as the high mass bin ($>0.07\ M_\odot$) is less than 0.02, with a $1-\sigma$ Bayesian confidence interval of $\epsilon_{bin1} - \epsilon_{bin2} = -0.34, -0.15$.

7.4. Brown Dwarf Binary Fraction as a Function of Age

By ages of 1 Gyr, most of our survey objects will have cooled to become T dwarfs. Thus, it is interesting to compare the primordial binary fraction of these objects to the binary fraction of similar objects in the field. Our survey is only sensitive to companions at projected separations of >10 AU, however, this is a particularly interesting separation space to probe, as older field T dwarf binaries rarely have separations this large (Burgasser et al. 2003, 2006). In fact, of the 32 T dwarfs surveyed in Burgasser et al. (2003, 2006), no companions were detected

Table 6
Statistical Sample Comparison as a Function of Mass

Sample 1	Sample 2	Likelihood	1σ CI on $\delta = \epsilon_{bin1} - \epsilon_{bin2}$	2σ CI on $\delta = \epsilon_{bin1} - \epsilon_{bin2}$
Upper Sco mass comparison (10–1000 AU separations)				
$<0.04\,M_\odot$	0.04–$0.1\,M_\odot$			
0/18, <9%	2/12, 17^{+15}_{-6}%	0.15	−0.28, −0.15	−0.42, 0.04
Upper Sco, Taurus, and Chamaeleon mass comparison (10–1000 AU separations)				
$<0.04\,M_\odot$	0.07–$0.1\,M_\odot$			
0/25, <7%	6/23, 26^{+11}_{-7}%	0.01	−0.34, −0.15	−0.44, −0.07
$<0.04\,M_\odot$	0.04–$0.07\,M_\odot$			
0/25, <7%	0/18, <9%	1.0	−0.06, 0.04	−0.15, 0.10
0.04–$0.07\,M_\odot$	0.07–$0.1\,M_\odot$			
0/18, <9%	6/23, 26^{+11}_{-7}%	0.03	−0.33, −0.13	-0.43, −0.04
Upper Sco, Taurus, Chamaeleon, and IC 348 mass comparison (30–1000 AU separations)				
$<0.04\,M_\odot$	0.07–$0.1\,M_\odot$			
0/36, <4.8%	3/43, 7^{+6}_{-2}%	0.25	−0.11, −0.02	-0.17, 0.03
$<0.04\,M_\odot$	0.04–$0.07\,M_\odot$			
0/36, <4.8%	0/20, <8%	1.0	−0.06, 0.02	−0.14, 0.07
0.04–$0.07\,M_\odot$	0.07–$0.1\,M_\odot$			
0/20, <8%	3/43, 7^{+6}_{-2}%	0.54	−0.10, 0.01	−0.16, 0.09

Table 7
Statistical Sample Comparison as a Function of Age

Sample 1	Sample 2	Likelihood	1σ CI on $\delta = \epsilon_{bin1} - \epsilon_{bin2}$	2σ CI on $\delta = \epsilon_{bin1} - \epsilon_{bin2}$
Upper Sco vs. field (10–1000 AU separations)				
$<0.04\,M_\odot$ BDs in Upper Sco	Field T Dwarfs			
0/18, <9%	0/32, <5%	1.0	−0.02, 0.07	−0.08, 0.15
Upper Sco, Taurus, and Chamaeleon vs. field (10–1000 AU separations)				
0.07–$0.1\,M_\odot$ Cluster BDs	Field M and L Dwarfs			
6/23, 26^{+11}_{-7}%	1/39, $2.6^{+5.4}_{-0.1}$%	0.01	0.14, 0.32	0.06, 0.43
Upper Sco, Taurus, Chamaeleon, and IC 348 vs. field (30–1000 AU separations)				
0.07–$0.1\,M_\odot$ Cluster BDs	Field M and L Dwarfs			
3/43, 7^{+6}_{-2}%	0/39, <4.4%	0.24	0.02, 0.11	−0.02, 0.17

with separation >10 AU (down to $q \geqslant 0.4$, i.e., comparable sensitivity limits to our survey). This places an upper limit on the binary fraction >10 AU of 5%. Again using the Fischer exact test method, we found a likelihood of 1 with a very tight $1-\sigma$ Bayesian confidence interval of $\epsilon_{bin1} - \epsilon_{bin2} = -0.02$, 0.07—i.e., given the small sizes of both of these samples, they are very likely drawn from the same parent sample. Thus, the very low mass brown dwarf binary fraction appears to be similar for both young and field objects. Binary fractions, likelihoods, and Bayesian confidence intervals between bins as a function of age are presented in Table 7.

Do higher mass objects ($>0.07\,M_\odot$) in young clusters also have a similar binary fraction (>10 AU) as their counterparts in the field? We compare the binary fraction (>10 AU separation) for 6 binaries discovered out of 23 young objects (the "high mass" bin from the previous section) drawn from binarity surveys of Upper Sco (Kraus et al. 2005), Taurus (Kraus et al. 2006; Konopacky et al. 2007), Chamaeleon (Ahmic et al. 2007), and this work with that of 1 binary (>10 AU separation) discovered from 39 field M8–L0.5 objects from Close et al. (2003). These two samples share a similar mass range (primary mass between 0.07 and 0.1 $M_\odot$), but very different wide binary fractions: 26^{+11}_{-7}% for the young sample versus $2.6^{+5.4}_{-0.06}$% for the old field sample. Using the Fischer exact test, the likelihood that

these two samples are drawn from the same binomial distribution is 0.01 with $1-\sigma$ Bayesian confidence interval of $\epsilon_{bin1} - \epsilon_{bin2} =$ 0.14, 0.32. Thus, for objects with mass $>0.07\,M_\odot$, there is an overabundance of 10–50 AU separation very low mass binaries in young clusters relative to the field.

Upper Sco is a somewhat older and higher density OB association, while Taurus and Chamaeleon are more diffuse, younger T clusters. Thus, we also compare binary fraction between these two different ages and environments. Combining the sample described in the previous section and separating by region, we find 3 binaries detected from 34 objects in Taurus and Chamaeleon and 3 binaries detected from 32 objects in Upper Sco. The binary fraction is nearly the same between the two, although it is important to note that the sample in Taurus and Chamaeleon has systematically higher primary masses than that in Upper Sco (dominated by the 18 very low mass brown dwarfs surveyed in this paper.) Thus, given the trend in binary fraction with mass, the binary fraction in Upper Sco may be considerably higher than in Taurus.

7.5. Trends in Very Wide Binarity (30–500 AU) as a Function of Age and Mass

We initially limited our statistical analysis to nearby clusters (<200 pc) since more distant clusters (e.g., NGC 1333, IC 348,

Serpens) are more than 250 pc distant and do not reach comparable sensitivity levels at separations of 10–30 AU. However, including results from surveys of these more distant clusters significantly boosts sample size. In particular, including the results from the Luhman et al. (2005) *HST* survey of IC 348 (2 Myr, 315 pc) introduces 31 additional $\leqslant 0.1\,M_\odot$ objects into this analysis. In order to match the achieved contrast and physical resolution of the Luhman et al. (2005) survey with those of nearer regions (Upper Sco, Taurus, Chamaeleon) we only consider results for separations from 30 to 500 AU.

Including objects from Luhman et al. (2005) in our three mass bins from earlier sections, we now find (1) in the high mass bin (0.07–0.1 $M_\odot$), 3 binaries are detected out of 43 objects surveyed (USco-55 and USco-66 from Kraus et al. 2005 and USco1609 from this work have separations <30 AU and thus would not be detected at the combined sensitivity limits for our composite survey), (2) in the medium mass bin (0.04–0.07 $M_\odot$), 0 binaries detected out of 20 objects surveyed, and (3) in the low mass bin (<0.04 $M_\odot$), 0 binaries detected out of 36 objects surveyed.

As before, the lowest mass cluster bin possesses a very similar upper limit on binarity as the field T dwarf bin and wide binaries seem to be rare in both the medium- and low-mass cluster bins. Comparing the high mass bin with the low mass bin, we find a likelihood of 0.25 that these two samples are drawn from the same binomial distribution, with a $1-\sigma$ Bayesian confidence interval of $\epsilon_{\mathrm{bin1}} - \epsilon_{\mathrm{bin2}} = -0.11, -0.02$. We also compare the high mass bin with the Close et al. (2003) sample (adjusting contrast levels, we now find 0 binaries imaged with separations >30 AU out of 39 surveyed objects). According to the Fisher exact test, the likelihood that these two samples were drawn from the same binomial distribution is 0.24 (as opposed to 0.01 for the same bin in the nearby sample.) Thus, a significant overdensity of young binaries relative to the field is apparent in this sample only at moderate separations (10–30 AU) and not at wide (30–500 AU) separations.

7.6. Stability of 10–50 AU Separation Binaries in Young Nearby Star-forming Regions

Up to ∼25% of very low mass (henceforth VLM) stars and substellar objects in young star-forming regions may have companions at separations >10 AU. However, very low mass star/brown dwarf binaries with separations >15 AU are rare in the field. Of ∼100 VLM binaries compiled at http://vlmbinaries.org, only ∼10% have separations >15 AU. Assuming a binary fraction of ∼10%, this means that less than 1% of field VLMs have companions at separations >15 AU (Close et al. 2007).

Close et al. (2007) suggest that very wide (>50 AU) young brown dwarf binaries are disrupted within the first 10 Myr of their existence by interactions with stars in their natal cluster. To set limits on the survival time of a young wide binary in its natal cluster, they adopt the analytic solution of Fokker–Planck coefficients from Weinberg et al. (1987) which describes the advective diffusion of a binary due to stellar encounters, namely, from this solution, the time t_* necessary to evaporate a binary with initial semimajor axis a_0 is

$$t_* \sim 3.6 \times 10^5 \left(\frac{n_*}{0.05\,\mathrm{pc}^{-3}} \right) \left(\frac{M_{\mathrm{tot}}}{M_\odot} \right) \left(\frac{M_*}{M_\odot} \right)^{-2}$$
$$\times \left(\frac{V_{\mathrm{rel}}}{20\,\mathrm{km\,s}^{-1}} \right) \left(\frac{a_\circ}{\mathrm{AU}} \right)^{-1}, \tag{12}$$

where n_* is the number density of stellar perturbers of mass M_* and relative velocity V_{rel}. Using this relationship, Close et al.

(2007) determine that young wide VLM binaries such as 2M 1207-39AB will not survive 10 Myr of interactions with 0.7 $M_\odot$ stellar perturbers with a number density n_* of 1000 pc^{-3}. Thus, Close et al. (2007) show that most of these binaries will not survive to join the field if born in a dense star-forming region. We determine here whether the same is true for moderately wide 10–50 AU binaries. While Close et al. (2007) assume a number density of nearby stars of 1000 pc^{-3}, which is appropriate near dense core regions, it is probably too high for objects in diffuse areas of Taurus or Chamaeleon. Assuming a typical density of 100 pc^{-3} for Taurus, Ophiuchus, and Upper Sco, we repeat this calculation for the six binaries that fall into our highest mass bin (specifically, CFHT-Tau 7, CFHT-Tau 17, and CFHT-Tau 18 from Konopacky et al. 2007; USco-55 and USco-66 from Kraus et al. 2005; and SCH 1609AB, the newly discovered binary presented herein). We find that all of these binaries are quite stable and will survive >10 Myr in either a 100 pc^{-3} environment or a 1000 pc^{-3} environment (i.e., long enough to join the field population). An environment with stellar densities >10^4 pc^{-3} (equivalent to the Trapezium cluster in Orion) is necessary to disrupt these binaries on <10 Myr timescales.

The existence of a significant population of these medium-separation binaries presents a conundrum, since very low mass stars and brown dwarf binaries with separations >15 AU are rare in the field. However, the field brown dwarf population encompasses a mix of objects which formed in a variety of different star-forming regions. Close et al. (2007) suggest that brown dwarf binaries with separations >20 AU are found rarely in the field because they can only form in low-density star-forming regions, while the majority of field objects formed in denser initial regions where any such binary would be disrupted. However, other authors have suggested that most stars in the field likely form in OB associations like Upper Sco (Konopacky et al. 2007; Preibisch & Mamajek 2008), so this is problematic.

The existence of this population of moderately wide young brown dwarf binaries in lower density young clusters initially suggests that most (predominantly single) field brown dwarfs must form in high stellar density regions which disrupt such wide binaries by late ages. However, this supposition relies on our ability to distinguish between "typical" versus "atypical" star-forming regions, as well as to truly disentangle the primordial versus evolved populations. In other words, the evolved population is the outcome of the formation mechanism plus any subsequent evolution in the cluster. Different combinations of formation and subsequent evolution may form the same evolved population. Here, we have placed constraints on binary evolution within a relatively diffuse cluster environment; placing constraints on formation mechanism is more difficult.

Forming brown dwarfs at all has always been a tricky prospect theoretically. Brown dwarf formation theories require either: (1) a mechanism to produce very low Jeans masses (e.g., turbulent fragmentation, gravitational fragmentation of infalling gas, and gravitational fragmentation with a magnetic field, Padoan & Nordlund 2004; Bate 2009; Bonnell et al. 2008; Price & Bate 2008) or (2) a method to circumvent the need for very low Jeans masses (e.g., ejection, or gravitational instability followed by binary disruption; Reipurth & Clarke 2001; Stassun et al. 2007; Stamatellos & Whitworth 2009). Unfortunately, more information is needed regarding the physical properties of these star-forming regions (i.e., measurement of turbulent motions, magnetic fields) to distinguish between these models. For instance, widespread filamentary structure has recently been observed by Herschel in very young star-forming clouds in

Aquila and Polaris (Men'shchikov et al. 2010). However, it is not currently clear what causes these filaments; if turbulence or magnetic fields are the dominant cause, this has significant ramifications for subsequent brown dwarf formation in these regions.

Likely a mix of formation mechanisms is at play in any given region, the detailed physics of which may vary from region to region. Disentangling these physics is a difficult prospect and requires more information than just binary fraction. While we can rule out pure ejection (without any dissipation from, e.g., a circumstellar disk) from our measured binary fraction and the existence of a significant population of >10 AU separation binaries, other models may produce a significant wide binary population which may be disrupted by late ages in dense clusters.

8. CONCLUSIONS

We searched for binary companions to 20 brown dwarfs in Upper Scorpius (145 pc, 5 Myr, nearest OB association) with the LGS AO and the facility infrared camera NIRC2 on the 10 m Keck II telescope. This survey is the most extensive to date for companions to very young (5 Myr), very low mass ($<40\,M_{\rm Jup}$) cluster brown dwarfs. We discovered a close companion ($0\farcs14$, 20.9 ± 0.4 AU) to the very low mass object SCH J16091837−20073523. From spectral deconvolution of integrated-light near-IR spectroscopy of SCH1609-2007 using the SpeX spectrograph (Rayner et al. 2003), we estimate primary and secondary spectral types of M6 $\pm$ 0.5 and M7 $\pm$ 1.0, corresponding to masses of $79 \pm 17\,M_{\rm Jup}$ and $55 \pm 25\,M_{\rm Jup}$ at an age of 5 Myr and masses of $84 \pm 15\,M_{\rm Jup}$ and $60 \pm 25\,M_{\rm Jup}$ at an age of 10 Myr.

For our survey objects with spectral types later than M8, we find an upper limit on binary fraction of <9% (1σ) at separations greater than 10 AU. As expected from similar mass binaries in the field, we find that the binary fraction (10–500 AU separations) appears to decrease monotonically with mass for young brown dwarfs. However, while proto-T-dwarfs ($M < 40\,M_{\rm Jup}$) have a similar wide (10–500 AU) binary fraction as field T dwarfs, there exists an anomalous population of wide higher mass binaries (0.07–$0.1\,M_{\odot}$ primaries, separations of 10–50 AU) at young ages relative to older ages.

REFERENCES

Ahmic, M., Jayawardhana, R., Brandeker, A., Scholz, A., van Kerkwijk, M. H., Delgado-Donate, E., & Froebrich, D. 2007, ApJ, 671, 2074

Allers, K. N. 2006, PhD thesis, Univ. of Texas
Allers, K. N., Kessler-Silacci, J. E., Cieza, L. A., & Jaffe, D. T. 2006, ApJ, 644, 364
Allers, K. N., et al. 2007, ApJ, 657, 511
Allers, K. N., et al. 2009, ApJ, 697, 824
Ardila, D., Martín, E., & Basri, G. 2000, AJ, 120, 479
Baraffe, I., Chabrier, G., Allard, F., & Hauschildt, P. H. 1998, A&A, 337, 403
Baraffe, I., Chabrier, G., Allard, F., & Hauschildt, P. H. 2002, A&A, 382, 563
Baraffe, I., Chabrier, G., Barman, T. S., Allard, F., & Hauschildt, P. H. 2003, A&A, 402, 701
Bate, M. R. 2009, MNRAS, 392, 590
Béjar, V. J. S., Zapatero Osorio, M. R., Pérez-Garrido, A., Álvarez, C., Martín, E. L., Rebolo, R., Villó-Pérez, I., & Díaz-Sánchez, A. 2008, ApJ, 673, L185
Bonnell, I. A., Clark, P., & Bate, M. R. 2008, MNRAS, 389, 1556
Bouchez, A. H., et al. 2004, Proc. SPIE, 5490, 321
Bouy, H., Brandner, W., Martín, E. L., Delfosse, X., Allard, F., Baraffe, I., Forveille, T., & Demarco, R. 2004, A&A, 424, 213
Bouy, H., Brandner, W., Martín, E. L., Delfosse, X., Allard, F., & Basri, G. 2003, AJ, 126, 1526
Brandeker, A., Jayawardhana, R., Khavari, P., Haisch, K. E., Jr., & Mardones, D. 2006, ApJ, 652, 1572
Brandner, W., et al. 2000, AJ, 120, 950
Briceño, C., Hartmann, L., Stauffer, J., & Martín, E. 1998, AJ, 115, 2074
Burgasser, A. J., Kirkpatrick, J. D., Cruz, K. L., Reid, I. N., Leggett, S. K., Liebert, J., Burrows, A., & Brown, M. E. 2006, ApJS, 166, 585
Burgasser, A. J., Kirkpatrick, J. D., Reid, I. N., Brown, M. E., Miskey, C. L., & Gizis, J. E. 2003, ApJ, 586, 512
Cameron, E. 2010, arXiv:1012.0566
Carpenter, B. 2009, LingPipe Blog: Natural Language Processing and Text Analytics, http://lingpipe-blog.com/2009/10/13/bayesian-counterpart-to-fisher-exact-test-on-contingency-tables/
Casali, M., et al. 2007, A&A, 467, 777
Chabrier, G., Baraffe, I., Allard, F., & Hauschildt, P. 2000, ApJ, 542, 464
Chauvin, G., Lagrange, A.-M., Dumas, C., Zuckerman, B., Mouillet, D., Song, I., Beuzit, J.-L., & Lowrance, P. 2005, A&A, 438, L25
Close, L. M., Siegler, N., Freed, M., & Biller, B. 2003, ApJ, 587, 407
Close, L. M., et al. 2007, ApJ, 660, 1492
Cruz, K. L., Kirkpatrick, J. D., & Burgasser, A. J. 2009, AJ, 137, 3345
Cushing, M. C., Vacca, W. D., & Rayner, J. T. 2004, PASP, 116, 362
Cushing, M. C., et al. 2008, ApJ, 678, 1372
de Bruijne, J. H. J., Hoogerwerf, R., Brown, A. G. A., Aguilar, L. A., & de Zeeuw, P. T. 1997, in ESA Symp., Hipparcos Venice '97, ed. R. M. Bonnet, et al. (ESA-SP 402; Noordwijk: ESA), 575
Diolaiti, E., Bendinelli, O., Bonaccini, D., Close, L., Currie, D., & Parmeggiani, G. 2000, A&AS, 147, 335
Dupuy, T. J., & Liu, M. C. 2010, ApJ, submitted
Dupuy, T. J., Liu, M. C., & Ireland, M. J. 2009, ApJ, 692, 729
Ghez, A. M., et al. 2008, ApJ, 689, 1044
Greissl, J., Meyer, M. R., Wilking, B. A., Fanetti, T., Schneider, G., Greene, T. P., & Young, E. 2007, AJ, 133, 1321
Guieu, S., Dougados, C., Monin, J.-L., Magnier, E., & Martín, E. L. 2006, A&A, 446, 485
Hambly, N. C., et al. 2008, MNRAS, 384, 637
Hewett, P. C., Warren, S. J., Leggett, S. K., & Hodgkin, S. T. 2006, MNRAS, 367, 454
Hodgkin, S. T., Irwin, M. J., Hewett, P. C., & Warren, S. J. 2009, MNRAS, 394, 675
Jayawardhana, R., & Ivanov, V. D. 2006, Science, 313, 1279
Joergens, V. 2006, A&A, 448, 655
Joergens, V., & Müller, A. 2007, ApJ, 666, L113
Joergens, V., Müller, A., & Reffert, S. 2010, A&A, 521, A24
Konopacky, Q. M., Ghez, A. M., Rice, E. L., & Duchêne, G. 2007, ApJ, 663, 394
Kraus, A. L., Ireland, M. J., Martinache, F., & Lloyd, J. P. 2008, ApJ, 679, 762
Kraus, A. L., White, R. J., & Hillenbrand, L. A. 2005, ApJ, 633, 452
Kraus, A. L., White, R. J., & Hillenbrand, L. A. 2006, ApJ, 649, 306
Lawrence, A., et al. 2007, MNRAS, 379, 1599
Liu, M. C., Leggett, S. K., Golimowski, D. A., Chiu, K., Fan, X., Geballe, T. R., Schneider, D. P., & Brinkmann, J. 2006, ApJ, 647, 1393
Lodieu, N., Hambly, N. C., Jameson, R. F., & Hodgkin, S. T. 2008, MNRAS, 383, 1385
Lodieu, N., Hambly, N. C., Jameson, R. F., Hodgkin, S. T., Carraro, G., & Kendall, T. R. 2007, MNRAS, 374, 372
Luhman, K. L. 2004, ApJ, 614, 398

Luhman, K. L., Mamajek, E. E., Allen, P. R., Muench, A. A., & Finkbeiner, D. P. 2009, ApJ, 691, 1265
Luhman, K. L., McLeod, K. K., & Goldenson, N. 2005, ApJ, 623, 1141
Martín, E. L., Delfosse, X., & Guieu, S. 2004, AJ, 127, 449
Men'shchikov, A., et al. 2010, A&A, 518, L103
Mohanty, S., Jayawardhana, R., Huélamo, N., & Mamajek, E. 2007, ApJ, 657, 1064
Padoan, P., & Nordlund, Å. 2004, ApJ, 617, 559
Preibisch, T., Brown, A. G. A., Bridges, T., Guenther, E., & Zinnecker, H. 2002, AJ, 124, 404
Preibisch, T., Guenther, E., Zinnecker, H., Sterzik, M., Frink, S., & Roeser, S. 1998, A&A, 333, 619
Preibisch, T., & Mamajek, E. 2008, in Handbook of Star Forming Regions, Vol. II, ed. B. Reipurth (The Southern Sky ASP Monograph Publications, Vol. 5; San Francisco, CA: ASP), 235
Preibisch, T., & Zinnecker, H. 1999, AJ, 117, 2381

Price, D. J., & Bate, M. R. 2008, MNRAS, 385, 1820
Rayner, J. T., Toomey, D. W., Onaka, P. M., Denault, A. J., Stahlberger, W. E., Vacca, W. D., Cushing, M. C., & Wang, S. 2003, PASP, 115, 362
Reipurth, B., & Clarke, C. 2001, AJ, 122, 432
Sivia, D. S., & Skilling, J. 2006, Data Analysis: A Bayesian Tutorial (Oxford: Oxford Univ. Press)
Slesnick, C. L., Hillenbrand, L. A., & Carpenter, J. M. 2008, ApJ, 688, 377
Stamatellos, D., Hubber, D. A., & Whitworth, A. P. 2007, MNRAS, 382, L30
Stamatellos, D., & Whitworth, A. P. 2009, MNRAS, 392, 413
Stassun, K. G., Mathieu, R. D., & Valenti, J. A. 2006, Nature, 440, 311
Stassun, K. G., Mathieu, R. D., & Valenti, J. A. 2007, ApJ, 664, 1154
Strom, K. M., & Strom, S. E. 1994, ApJ, 424, 237
Todorov, K., Luhman, K. L., & McLeod, K. K. 2010, ApJ, 714, L84
Vacca, W. D., Cushing, M. C., & Rayner, J. T. 2003, PASP, 115, 389
Weinberg, M. D., Shapiro, S. L., & Wasserman, I. 1987, ApJ, 312, 367
Wizinowich, P. L., et al. 2004, Proc. SPIE, 5490, 1